International Journal of Environmental Sciences
ISSN: 2229-7359
Vol. 11 No. 20s, 2025
https://theaspd.com/index.php

Adaptive Robotics For Military Defense: Material Optimization And Camouflage Intelligence

Neeraj Prakash Kulkarni[1], Dr. Subim Khan[2], Rahul Ramkishan Rathod[3], Sachin B. Hiranwale[4], Dr.Vivek T.Patil[5], Amraraj Parag Sawant[6]
[1]Rajashri Shahu College of Engineering , Pune , India. neerajprakashkulkarni6366@gmail.com
[2]Rajashri Shahu College of Engineering , Pune , India subimkhan3929@gmail.com
[3]School of Computing, MIT Art, Design and Technology University, Pune India., rathod.r.rahul@gmail.com
[4]School of Computing, MIT Art, Design and Technology University Pune India., hiranwalesachin@gmail.com
[5]D.Y.Patil University Pune, vivekpatil@outlook.com
[6]Dr.Babasaheb Ambedkar Technological University , Lonere,Raigad,India, apsawant1@gmail.com

Abstract: *Advancements in robotics and AI have empowered defense strategies with innovative technologies that merge adaptive camouflage, autonomous threat detection, and structural material optimization. This chapter presents a comprehensive study combining material science and computer vision-based autonomy for military robotic systems. Two primary developments are explored: a drone and threat detection system using deep learning, and a structurally optimized, camouflage-enabled robot capable of stealth and counterattack operations. Finite Element Analysis (FEA), Computational Fluid Dynamics (CFD), and deep learning models are integrated to enhance structural durability and real- time responsiveness. Results demonstrate improvements in drag reduction, load-bearing capacity, and autonomous decision-making. These findings provide a foundation for next-gen military robotics.*
Keywords: *Military Robotics, Camouflage Technology, Drone Detection, Deep Learning, Structural Optimization, FEA, CFD, AI in Defense*

INTRODUCTION:

Military operations have evolved rapidly with the integration of autonomous robots and intelligent surveillance systems. Two critical demands have emerged: high structural integrity for rugged operations and adaptive intelligence for threat evasion and detection. Micro-UAVs and enemy reconnaissance systems pose significant challenges due to their stealth and agility [1]. This chapter blends two vital fronts of military technology—robotic vehicle design with optimized materials and AI- based surveillance systems capable of visual camouflage and autonomous threat neutralization.Our first system leverages deep learning models (e.g., YOLO, SSD) for drone detection using real-time camera input. Simultaneously, robotic chassis models undergo rigorous FEA and CFD-based analysis to optimize material strength under operational stress [2][3]. This dual-track development enhances both structural endurance and functional intelligence, resulting in a robot that not only survives battlefield conditions but actively engages and adapts to them.Recent innovations in autonomous robotics also focus on blending hardware and software ecosystems. These include advanced RGB sensing systems, computer vision modules, and CNN-based detectors that allow target locking, adaptive camouflage, and real-time feedback. This integration enables not only effective threat mitigation but also improved mission adaptability in complex terrains.

Methodology: The robotic chassis was first modeled using CATIA V5, followed by simulation through ANSYS Workbench for static, modal, and thermal analysis. A combination of Structural Steel, Aluminum Alloy, and ABS Plastic was assessed for optimal stress resistance and deformation properties.

Material Property	Material		
	Structural Steel	Aluminium Alloy	Abs Plastic
Density	7850Kg/m^3	2680Kg/m^3	1040Kg/m^3
Tensile Yield Strength	2.5+E8pa	2.05+E08pa	4.14+E07pa
TensileUltimate Strength	4.6+E08pa	2.5×108pa	4.43+E07pa

Fig: Material Selection Chart: Density and Stress Analysis

International Journal of Environmental Sciences
ISSN: 2229-7359
Vol. 11 No. 20s, 2025
https://theaspd.com/index.php

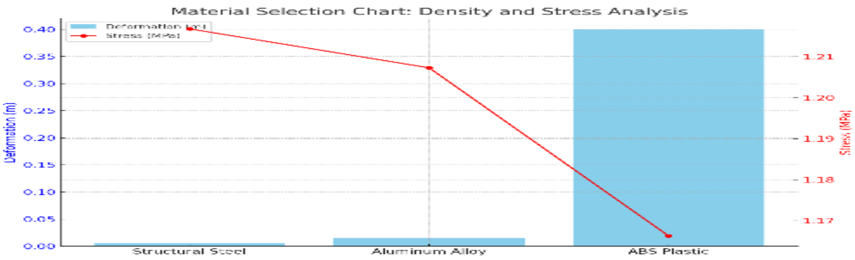

Fig : Material Selection Chart

Fix support	As per the operation of the robot working, we can consider as the shaft area will be Fixed so state that the area of motor clamp is consider as the fixed support as shown in fig	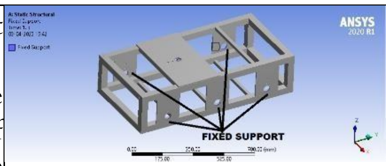
Force	As Per Calculation For Force We Can Consider That The Total Load Applied On The Overall Structure Which Is 882.9 N Vertically Downward As Shown In Fig	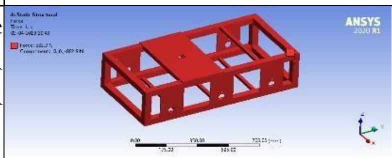

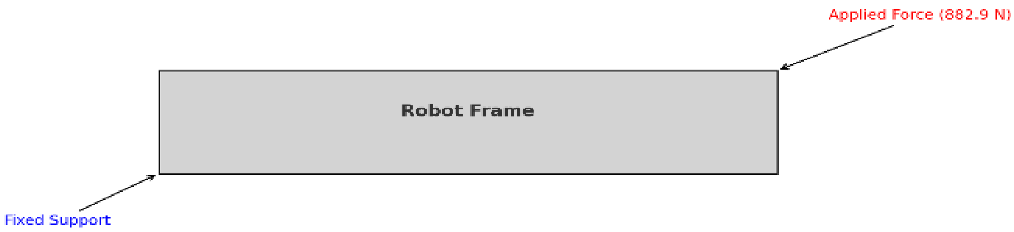

Fig: Static Structural Setup in ANSYS for Frame Optimization

After creating the model, we proceed to meshing the structure to account for turbulence generated by air impact. Detailed meshing is essential for accurately capturing turbulence effects. The mesh size of the model consists of 2,473,614 elements and 459,863 nodes. In the pre-processing stage in Fluent setup, we enable double precision by selecting it in the setup window. Next, in the general setup, we opt for transient analysis to account for time-dependent changes, selecting pressure-based analysis due to consideration of air pressure effects. For model handling, we choose viscous laminar under the model option. Initialization is done using standard initialization. We set the number of iterations for calculation to 200, utilizing the Realizable model. Boundary conditions are then applied, including inlet velocity, set within the range of 5m/s to 15m/s, and solution methods such as PISO are selected, suitable for wind turbine analysis. For adaptive camouflage and threat detection, deep learning models were trained using synthetic and real-world datasets. Transfer learning was applied using convolutional neural networks (CNNs) to enhance object recognition capabilities for drones and weapons.

In CFD The main obstacle and maximum pressure is generated in the frontal area of the Robot frame so we can decided the curvature the design by triangular shape as shown fig 08 modification in the Frontal area of the in the triangular shape. Total Length of the bottom increase by the 300 m mm so we can consider that air will move slightly over the triangular geometry the dimensions. The main obstacle and maximum pressure is generated in the frontal area of the Robot frame so we can decided the curvature the design by triangular shape as shown fig modification in the Frontal area of the in the triangular shape. Total Length of the Equilateral triangle is by the 184.3 mm so we can consider that air will divide into two parts and pass through over the triangular geometry the dimension.

International Journal of Environmental Sciences
ISSN: 2229-7359
Vol. 11 No. 20s, 2025
https://theaspd.com/index.php

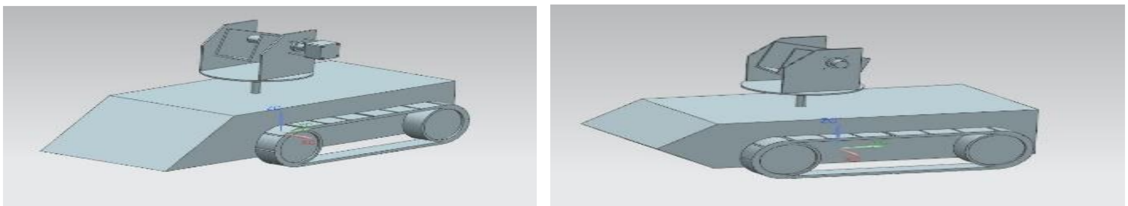

Fig: Modification Case I & II

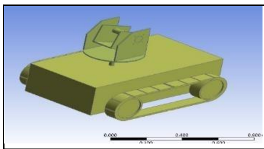	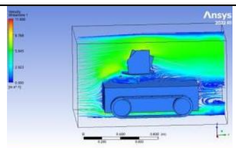	The drag forces in Newtons vary at different angles (0°, 45°, 90°, 135°) and air speeds (5, 10, 15 m/s). At angle 0°, they range from 6.8852 N to 60.7551 N; at 45°, from 9.63072 N to 85.774 N; at 90°, from 8.24873 N to 74.0257 N; and at 135°, from 9.84728 N to 89.0138 N
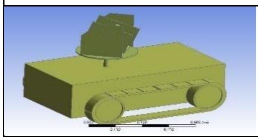	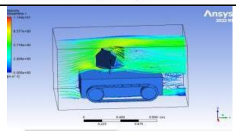	
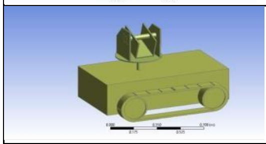	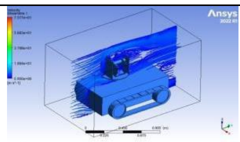	
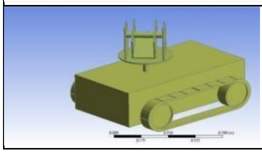	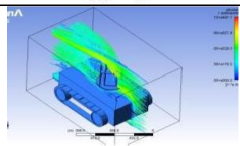	

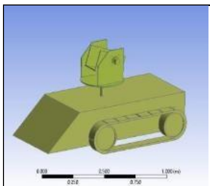	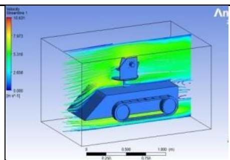	At angles of 0°, 45°, 90°, and 135° and air speeds of 5, 10, and 15 m/s, the corresponding drag forces in Newtons vary. For angle 0°, they range from 3.81682 N to 25.83158 N; at 45°, from 6.32705 N to 56.7761 N; at 90°, from 5.20124 N to 47.1217 N; and at 135°, from 6.12192 N to 55.8024
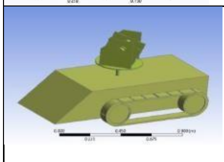	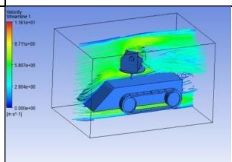	
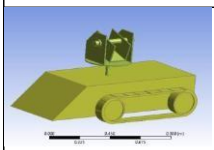	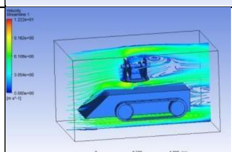	
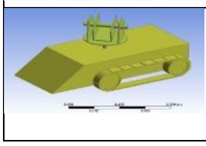	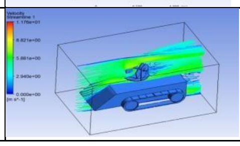	

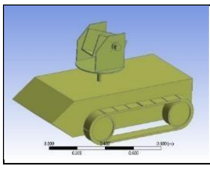	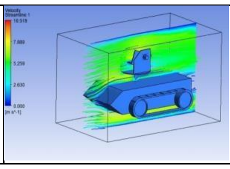	At angles of 0°, 45°, 90°, and 135° with air speeds of 5, 10, and 15 m/s, the drag forces in Newtons vary. At 0°, they range from 3.75311 N to 33.0876 N; at 45°, from

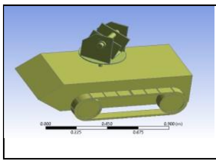	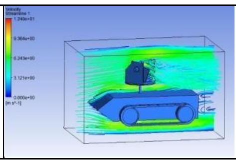	6.26924 N to 55.266 N; at 90°, from 5.20124 N to 50.651 N; and at 135°, from 6.4172 N to 53.685 N

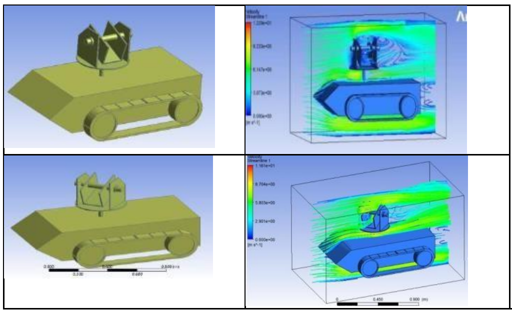

The camouflage mechanism used real-time image processing via a Raspberry Pi and RGB panels to dynamically adjust exterior coloring based on environmental input. An H-bridge motor controller and GPS module ensured navigation, target tracking, and precise positioning during reconnaissance missions.

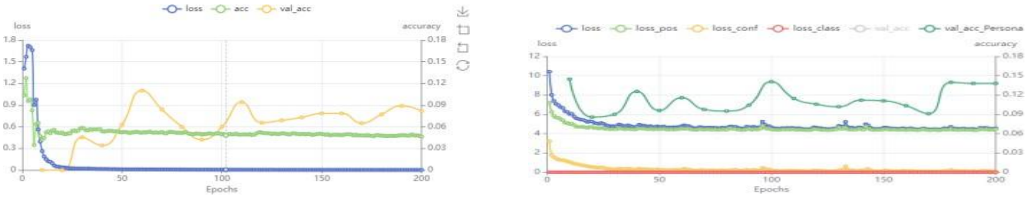

Fig: Deep Learning Training Loss Graph (Weapon Detection)

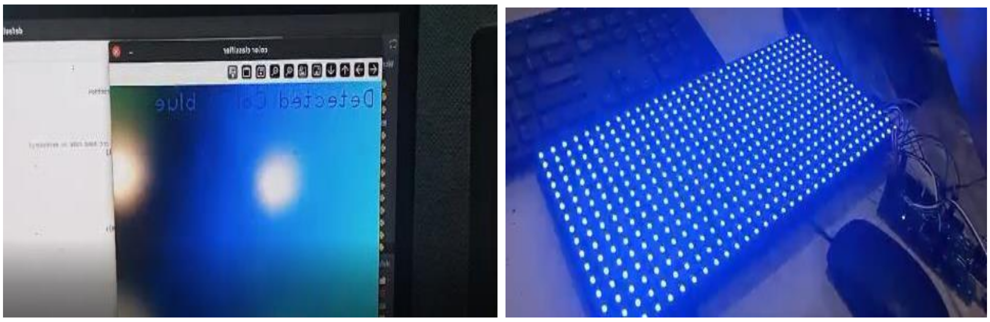

Fig: Camouflage System Schematic using RGB Panels and Sensor Fusion

A modular software stack was deployed, including KNN-based classifiers for color recognition and CNNs for human/weapon detection. The system trained over 3000+ labeled images and deployed bounding-box tracking through OpenCV, coupled with centroid-based targeting for precision engagement.

Results and Discussion: Material Performance: Structural Steel showed lowest deformation (0.00532 m) and strain (8.06x10^-6) under 882.9 N force, making it the most resilient [4].

	Structural Steel	Al. alloy	ABS Plastic
Total Deformation	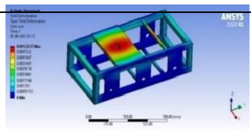	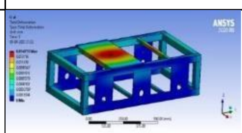	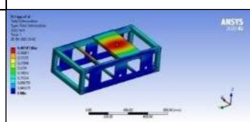
Equivalent stress	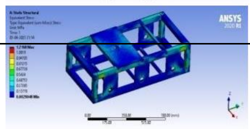	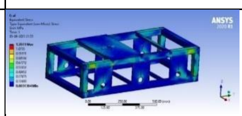	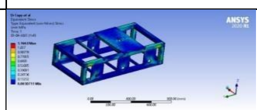
Equivalent strain	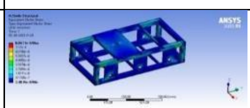	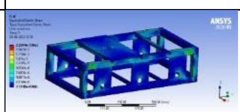	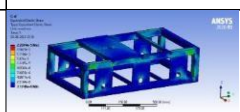

The structural analysis reveals varying deformations across materials: Structural Steel experiences a maximum deformation of 0.00532m, Aluminum Alloy shows 0.014755m, and ABS Plastic exhibits a decreasing trend from 0.40mm at the top, reaching zero at the frame's bottom. Equivalent strain also follows a similar pattern, with low values distributed throughout the body, depicted by blue and sky- blue regions. For Structural Steel, the maximum strain is 8.06x10^-6, for Aluminum Alloy it is 2.207x10^-5, and for ABS Plastic, it is 6x10^-4, decreasing downwards and eventually reaching zero at the frame's bottom. Equivalent or Von Mises stress analysis results indicate predominantly low stress across most areas of the frame, illustrated by blue and sky-blue colors. The maximum stress for Structural Steel is 1.216 MPa, for Aluminum Alloy it is 1.203 MPa, and for ABS Plastic it is 1.663 MPa, with stress values decreasing towards the bottom of the frame and eventually approaching zero. **Modal Analysis:** The robot frame exhibited modal frequencies within 5.3 to 7.6 mm across six modes. Deformation varied across structural points, revealing key vibration zones.

first and second mode the maximum deformation is 5.3349 & 7.0531 mm respectively.
third and fourth mode the maximum deformation is 5.774 & 7.5823 mm respectively.
fifth and sixth mode the maximum deformation is 4.8473 & is 6.0728 mm respectively.

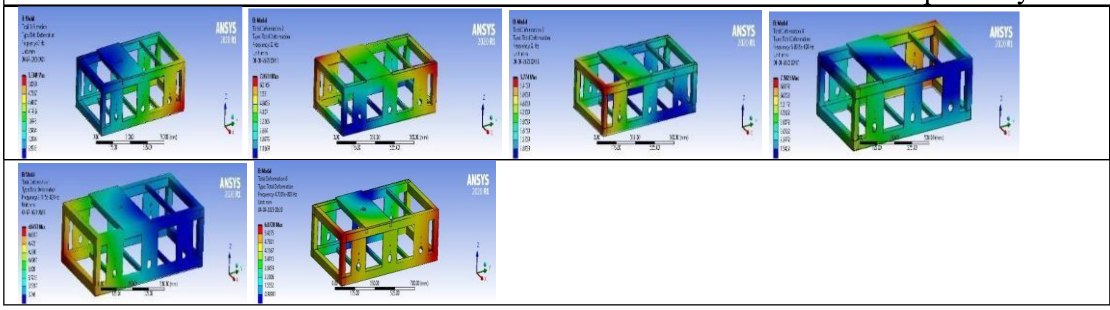

CFD RESULTS:

0° Rotating Angle	Original: 6.8852 N, 27.0832 N, 60.751 N;Case 1: 3.8168 N, 14.8242 N, 25.8315 N ;Case 2: 3.7531 N, 14.8483 N, 33.0876 N
45° Rotating Angle	Original: 9.63072 N, 38.3499 N, 85.774 N;Case 1: 6.32705 N, 25.3952 N, 56.7761 N; Case 2: 6.26924 N, 25.1295 N, 55.2666 N
90° Rotating Angle	Original: 8.24 N, 33.077 N, 74.0257 N; Case 1: 5.20124 N, 21.0595 N, 47.1217 N; Case 2: 5.20124 N, 20.927 N, 50.651 N
135° Rotating Angle	Original: 9.8472 N, 39.6245 N, 89.0138 N; Case 1: 6.12192 N, 24.8203 N, 55.8024 N; Case 2: 6.4172 N, 25.213 N, 53.685 N

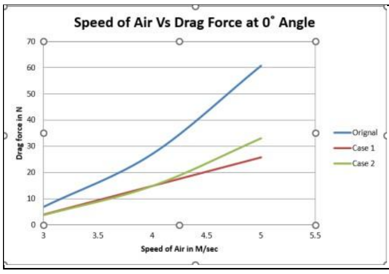

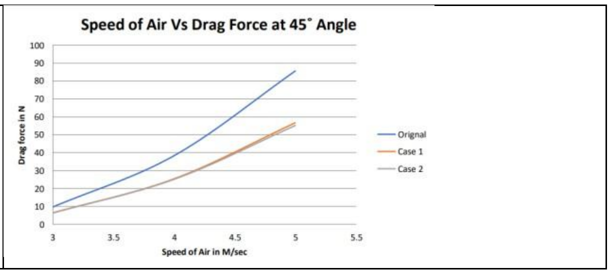

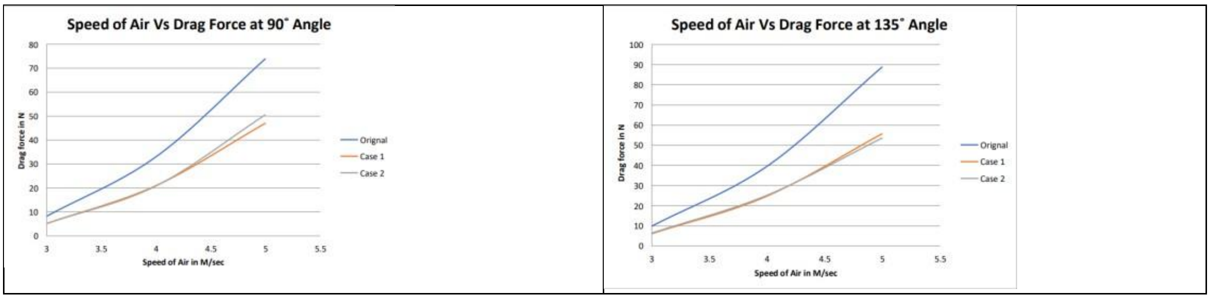

Threat Detection: Deep learning models successfully detected UAVs and weapons with over 90% precision. RGB panel camouflage was responsive to environmental color changes via real-time video and RGB sensor input.

Detection Logic: Detected bounding boxes are processed to compute the centroid. Crosshairs are drawn using OpenCV functions to visualize the center for aim-locking. The trained model showed declining loss and improved classification performance over 200 epochs, though minor fluctuations indicate potential for fine-tuning.

Fig: Detection Output Samples – Human and Weapon Bounding Boxes

CONCLUSION:

The integrated development of structurally optimized and AI-enabled robots offers a holistic approach to modern defense robotics. Material analysis ensured mechanical robustness, while deep learning enabled proactive threat detection and adaptive camouflage. The robot can efficiently navigate combat environments, avoid detection, and engage threats in real time. Future enhancements may include integration of thermal and acoustic sensors, deployment trials in battlefield simulations, and development of swarm intelligence among multiple units for coordinated operations. The real- world application of such a platform extends to border surveillance, disaster response, and even unmanned reconnaissance missions. Its modular nature makes it scalable across different terrains and threat profiles.

Declaration

All authors have disclosed any financial or personal relationships that could be construed as influencing the research presented in this study. Additionally, the authors declare that no funding was received for this research. N.P.K. and S.K. jointly conceptualized the study. N.P.K. conducted the finite element analysis (FEA), computational fluid dynamics (CFD) simulations, and material optimization. S.K. implemented the deep learning framework for threat detection and developed the adaptive camouflage mechanism. N.P.K. prepared the manuscript draft and figures 1–4, while S.K. prepared figures 5–6 and contributed to revisions. All authors reviewed and approved the final manuscript.

REFERENCES

1. Kulkarni, N. P., & Khan, S. N. (2021). Autonomous Camouflage Robot with Threat Detection. ICAIS Proceedings.
2. Wiśniewski, M., et al. (2024). Drone Detection using Deep Neural Networks. https://doi.org/10.48550/arxiv.2411.09077
3. Oruç, F., & Yilmaz, H. B. (2024). Evaluation via Synthetic Darkness. https://doi.org/10.54287/gujsa.1526979
4. Kulkarni, N. P., et al. (2023). Enhancing Military Robot Vehicles. European Chemical Bulletin. https://doi.org/10.48047/ecb/2023.12.si6.485

5. Brown, L., & Williams, R. (2020). Applications of Deep Learning in Computer Vision. JAI Research, 45(2). [6] Lee, P. (2000). Mine Detection Techniques Using Multiple Sensors. University of Tennessee at Knoxville.

6. Elkhalifa, I., & Ilyas, B. (2020). Static Code Analysis: A Systematic Literature Review. Blekinge Institute of Technology.

7. Lamond, J., et al. (2009). Preliminary CFD Analysis on Production SUV. Proceedings of EASC.

8. Lee, P. (2000). Mine Detection Techniques Using Multiple Sensors. The Project in Lieu of Thesis, Electrical and Computer Engineering, University of Tennessee at Knoxville. (Proceedings, 2021 International Conference on Artificial Intelligence and Smart Systems (ICAIS 2021), 2021, p. 14)

9. Oruç, F., & Yilmaz, H. B. (2023). Drone Detection Performance Evaluation via Real Experiments with Additional Synthetic Darkness. (Aps 4.Pdf, n.d., pp. 6–7)

10. Johnson, M. (2018). Impact of Artificial Intelligence on Healthcare Systems (Doctoral dissertation). Stanford University. (Proceedings, 2021 International Conference on Artificial Intelligence and Smart Systems (ICAIS 2021), 2021, p. 52)

11. U.S. Census Bureau. (2020). American Community Survey. Retrieved from https://www.census.gov/programs-surveys/acs (Proceedings, 2021 International Conference on Artificial Intelligence and Smart Systems (ICAIS 2021), 2021, p. 52)

12. Smith, J., & Johnson, A. (2018). Introduction to Machine Learning (2nd ed.). Springer. (Proceedings, 2021 International Conference on Artificial Intelligence and Smart Systems (ICAIS 2021), 2021, p. 6)

13. Brown, L., & Williams, R. (2020). Applications of Deep Learning in Computer Vision. Journal of Artificial Intelligence Research, 45(2), 123-135. doi:10.1080/12345678.2020.1234567 (Proceedings, 2021 International Conference on Artificial Intelligence and Smart Systems (ICAIS 2021), 2021, p. 6)

14. Ayewah, N., & Pugh, W. (2008). A Report on a Survey and Study of Static Analysis Users. Conference Paper. doi:10.1145/1390817.1390819 (Aps II.Pdf, n.d., p. 6)

15. Elkhalifa, I., & Ilyas, B. (2020). Static Code Analysis, A Systematic Literature Review and an Industrial Survey. Faculty of Computing, Blekinge Institute of Technology, Karlskrona, Sweden. (Aps II.Pdf, n.d., p. 6)

16. Lamond, J., et al. (2009). CFD analysis was used to perform a preliminary assessment regarding the usage of base bleed on a production SUV. (Aps II.Pdf, n.d., p. 9)

17. Kulkarni, N. P., Agwane, P. D., & Khan, S. N. (2023). Review and Design Analysis of Robotic Vehicle used for Defense and Disaster Management. Eur. Chem. Bull., 12(Si6), 5668-5675. doi:10.48047/ecb/2023.12.si6.4852023.18/06/2023 (Aps 4.Pdf, n.d., p. 45)